Stokes flow,

$$f_{Br} = 6\pi\mu a\, l\, v_p, \tag{1}$$

$$l = \frac{4}{3}\sinh\alpha \sum_{n=1}^{\infty} \frac{n(n+1)}{(2n-1)(2n+3)} \times \left(\frac{2\sinh(2n+1)\alpha + (2n+1)\sinh 2\alpha}{4\sinh^2(n+1/2)\alpha - (2n+1)^2 \sinh^2\alpha} - 1 \right),$$

where a is the radius of the sphere, $\alpha = \cosh^{-1}(z/a)$ and z is the distance between the center of the sphere and the wall.

Cox and Brenner(1967) also proposed the model of fluid force in the near-wall region considering the effect of fluid inertia,

$$f_C = 6\pi\mu a v_p \frac{1}{\varepsilon}\left[1 + \frac{1}{5}\left(1 + \frac{Re_p}{2}\right)\varepsilon \ln\frac{1}{\varepsilon}\right], \tag{2}$$

where $Re_p\,(= \rho_f v_p a/\mu)$ is the particle Reynolds number, $\varepsilon = l_{app}/a$ and $l_{app}\,(= z-a)$ is the minimum distance between surfaces.

Considering only the effect of squeezed fluid, the lubrication force caused by the interstitial pressure is obtained (Adams ,1985),

$$f_L = 6\pi\mu a^2 v_p / l_{app}\,. \tag{3}$$

Eqs.(2) and (3) are valid for the condition of the Reynolds number defined by the approach distance, $Re_g\,(= \rho_f v_p l_{app}/\mu) << 1$.

It is known that the added mass force is also changed near the wall and given by

$$f_A = m' \frac{dv_p}{dt} + \frac{1}{2}\frac{dm'}{dt} v_p, \tag{4}$$

$$m' = \frac{2}{3}\pi\rho_f a^3 \left(1 + \sum_{i=0}^{\infty} \frac{3a^{3(i+1)}}{f_0 f_1 \cdots f_i}\right),$$

where $f_0 = 2z$, $f_i = 2z - a^2/f_{i-1}$ (Soo,1967)

NUMERICAL METHODS

Basic equations for an incompressible fluid flow described in general curvilinear coordinates are as follows,

$$\frac{\partial J}{\partial t} + \frac{\partial (JU^j)}{\partial x^j} = 0, \tag{5}$$

$$\frac{\partial (Ju_i)}{\partial t} + \frac{\partial}{\partial x^j}(JU^j u_i) + J\frac{\partial x^j}{\partial x_i}\frac{\partial P}{\partial x^j} - \nu\frac{\partial}{\partial x^k}\left(\frac{\partial x^k}{\partial x_j}\frac{\partial}{\partial x^l}\left(J\frac{\partial x^l}{\partial x_j}u_i\right)\right) = 0, \tag{6}$$

$$U^j = \frac{\partial x^j}{\partial t} + \frac{\partial x^j}{\partial x_i}u_i, \tag{7}$$

where $Jacobian\ J = \left|\partial x_i/\partial x^j\right|$. The velocity components of the fluid u_i are defined in rectangular coordinates x_i. In general coordinate system x^j, the contravariant velocity U^j which includes the grid velocity $\partial x^j/\partial t$, is used for expressing the convective flux of momentum.

The local grid velocity at the cell boundary in computational space is given by Eq.(8) and must satisfy the geometry conservation law given by Eq.(9) at each cell,

$$\frac{\partial x^j}{\partial t} = -\frac{\partial x^j}{\partial x_i}\frac{\partial x_i}{\partial t}, \tag{8}$$

$$\frac{\partial J}{\partial t} + \frac{\partial}{\partial x^j}\left(J\frac{\partial x^j}{\partial t}\right) = 0. \tag{9}$$

The translational and the rotational motion of the particle are calculated by the equations of motion expressed as Eqs.(10) and (11), respectively. The fluid force acting on the particle is calculated directly by integrating the stress and the pressure on the surface without any models,

$$m_p \frac{d\boldsymbol{v_p}}{dt} = \int_{S_p} (\boldsymbol{t}\cdot\boldsymbol{n})\,\boldsymbol{n}\,dS + \boldsymbol{F_g}, \tag{10}$$

$$I_p \frac{d\boldsymbol{\omega_p}}{dt} = \int_{S_p} (r_p \boldsymbol{n}\times\boldsymbol{t})\,dS, \tag{11}$$

where m_p is the mass of a particle, I_p is the moment of particle inertia and $\boldsymbol{\omega_p}$ is the rotational velocity. $\boldsymbol{t}$ is the stress vector on the particle surface S_p and $\boldsymbol{n}$ is the normal unit vector on S_p. $\boldsymbol{F_g}$ is the gravity and the buoyancy force.

The calculation method of fluid flow is based on the fractional-step method. The algebraic method was applied to grid generation in order to express the continuous change of grid system in time. We adopted an *L-type* grid in the present calculation. The collocated method is applied to the discretization of the fluid calculation. The variables of the fluid flow are defined at the center of each cell except for the contravariant velocity U^j, which is defined at the boundary of the cell.

EXPERIMENT

The trajectory and the velocity of a particle falling toward a horizontal wall were investigated experimentally at the same conditions as the numerical simulation. A spherical nylon particle, on which a small piece of thin iron film was attached, was fixed magnetically by a DC solenoid attached to a positioning device near a horizontal plane wall in a tank filled with silicone,

Table 1 Experimental conditions and corresponding dimensionless parameters for numerical simulation

		Case a	Case b
ρ_p	[kg/m^3]	1131	1127
D_p	[mm]	12.7	25.4
ρ_f	[kg/m^3]	983 (at 9°C)	985 (at 7°C)
μ	[kg/m·s]	0.134 (at 9°C)	0.142 (at 7°C)
U_t	[cm/s]	6.47	14.6
l_{ini}	[mm]	2.95	5.31
ρ_p/ρ_f		1.150	1.144
Re_t		6.01	25.8
Fr_t		0.0336	0.0858

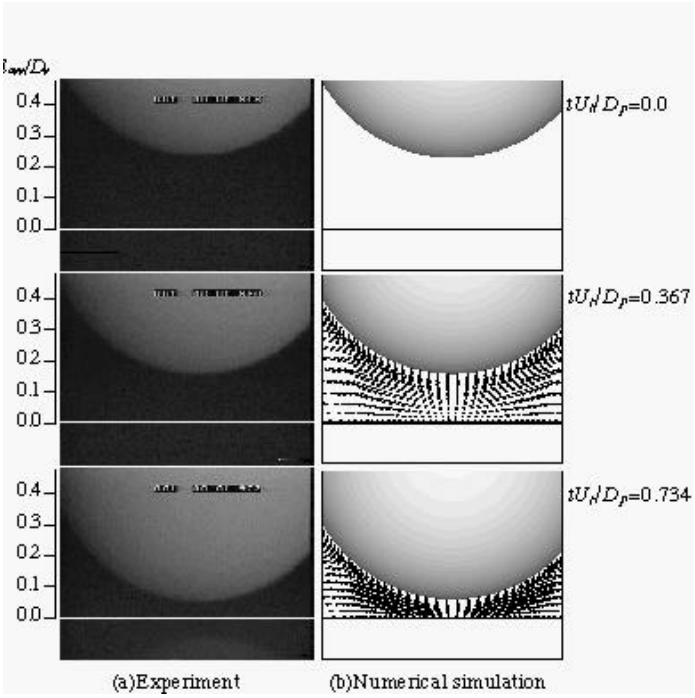

Fig.1 Instantaneous particle and fluid motions for Case a

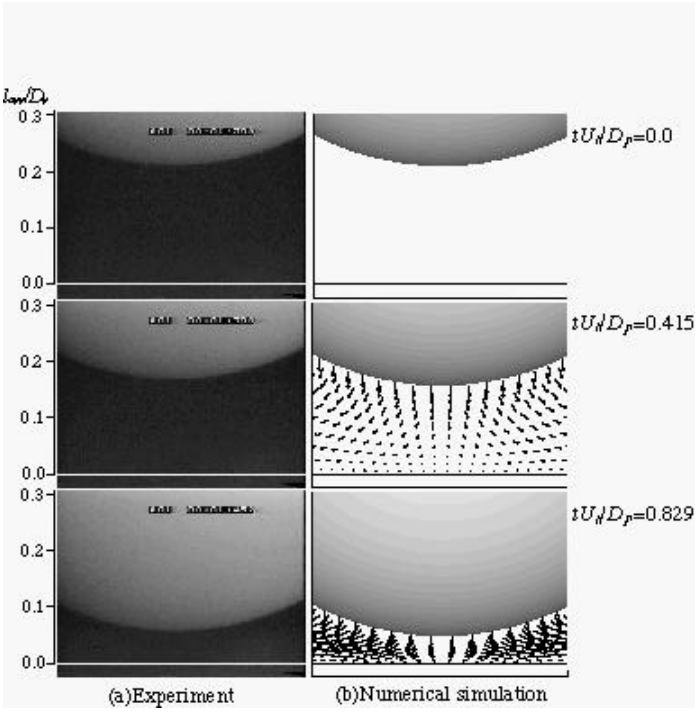

Fig.2 Instantaneous particle and fluid motions for Case b

and was released from the solenoid The images of the particle motion were recorded with a high-speed video camera. The sedimentation velocity was calculated from the obtained approach distance as a function of time. Table 1 shows the experimental conditions and the corresponding dimensionless parameters for numerical simulation, where r_p is the density, D_p is the diameter, U_t is the terminal velocity of a particle, l_{ini} is the initial approach distance and Re_t, Fr_t are the Reynolds number and the Froude number calculated by U_t respectively. The properties of silicone are largely dependent on the temperature, so that the density and the viscosity of the fluid were corrected at every experiment.

RESULTS

Figs.1 and 2 show the sequences of snapshots of the particle motion. In these figures, the numerical and the experimental results are compared in the same reduces scale. It was able to be simulated until the approach distance reached about 5% of the diameter. Regarding the motion of the particle, the numerical simulations give good predictions. The numerical results also show the velocity profile of the fluid in a cross section of the center of the gap. The draining flow from the gap shows the symmetrical motion, and the parabolic profile along the wall have been observed as the approach distance is decreased. These features of the fluid flow imply that the momentum transfer in the gap is dominated by viscous diffusion normal to the wall, as is assumed in the lubrication theory.

Fig.3 indicates the approach distance l_{app}/D_p as a function of normalized time, and Fig.4 (a), (b) are the relation between

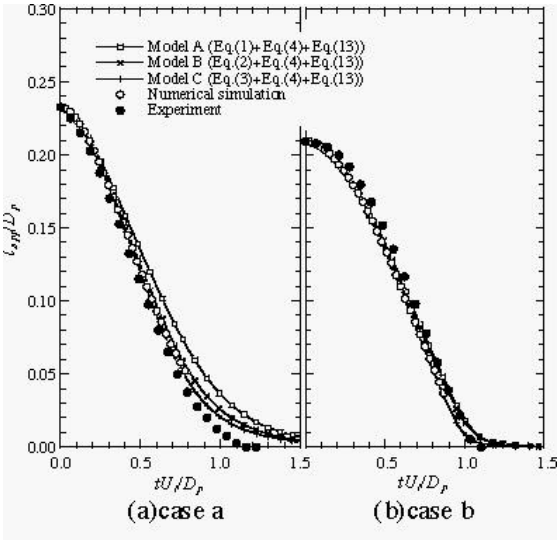

Fig.3 Trajectories of a particle falling toward a wall in fluid

approach distance and the normalized approach velocity of the particle toward the wall v_p/U_t. Davis (1986) defined the Stokes number which express the ratio of the particle inertia to the viscous force near the wall,

$$St = \frac{r_p v_l D_p}{9m}, \qquad (12)$$

where v_l is the approach velocity near the wall. Using the particle velocity at $l_{app} = 0.1D_p$ as v_l, $St = 0.22$ and 0.92 in *Cases a*

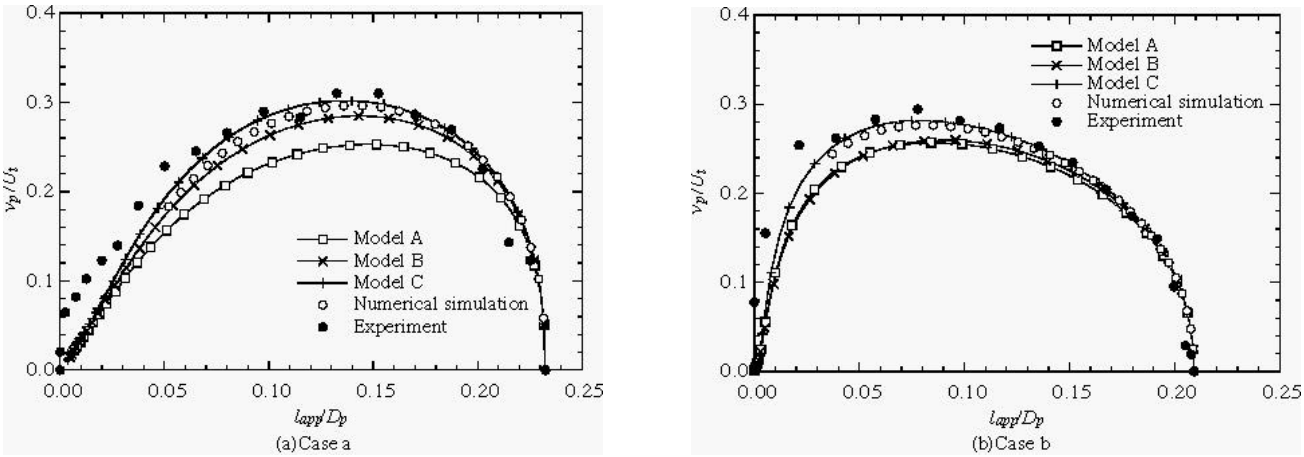

Fig.4 Relations between approach distance and approach velocity

and *b*, respectively. Comparing both cases with respect to the particle velocity in Fig.4, we found that the particle come into deceleration at the further point from the wall in the case of less St. Solid lines in Fig.4 show the analytical results of thee fluid force models. All models contain the steady force(Eqs.(1)~(3) are used in Model A~C, respectively), the added mass force(Eq.(4)) and the Basset history force given by

$$f_{Ba} = 6a^2\sqrt{\pi\rho_f\mu}\int_{-\infty}^{t}\frac{dv_p/dt'}{\sqrt{t-t'}}\,dt' \quad . \tag{13}$$

In Figs.3 and 4, these models show the good agreement with the experimental and the numerical ones, except for the near-wall region ($l_{app}/D_p < 0.05$).

Fig.5 shows the pressure profiles along the wall for *Cases a* and *b* at the approach distance, about 5% of the diameter. The solid line indicates the corresponding results derived from lubrication theory. Both cases show nearly the same profile, which takes the maximum at the center and goes to zero asymptotically with increasing the distance from the center. Especially in *Case a*, the numerical results agree with theoretical ones quantitatively. However, their results could not be compared strictly, because the lubrication theory is derived on the assumption that the particle approaches to the wall with constant velocity and so it does not include the effect of the particle unsteady motion.

Fig.6 shows the transition of each component and fluid force by Model A~C made up of the components. The set of components for each model is shown in the legend of Fig.3. The components of the models, except for the Basset history force, were calculated by using the particle velocity and the acceleration at the corresponding position obtained by the simulation. The Basset history force was evaluated by integrating the acceleration with respect to time numerically. Because the simulated results are not available in the neighborhood of the wall, we numerically integrated the equation of motion with Models B and C in *Cases a* and *b*, respectively. The dashed lines indicate these results in Fig.6.

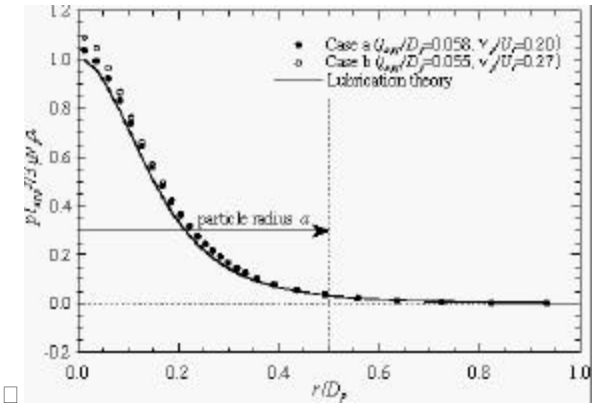

Fig.5 Pressure distribution along the wall

At the moment the particle set in motion from an initial state, the two unsteady fluid forces, the added mass force and the Basset history force, are dominant, and the simulation results agree with the sum of them in both cases. As the particle approaches to the wall, the steady fluid force is increased with the increase of the velocity, and the unsteady forces are decreased with the decrease of the acceleration. In both cases, the fluid force exceeds the gravity around $l_{app}/D_p = 0.1$ and, after that, the particle is decelerated and the added mass force changes its direction. In the case of large St, large approaching velocity remains up to the neighborhood of the wall, so that the sudden increase of the steady component appears.

These figures also show that the Basset history force has an innegligible effect on the particle motion through the sedimentation in both cases. However, these unsteady effects become minor as the particle approaches to the wall, so that the pressure distributions shown in Fig.5 would agree with the theoretical one that assumes a steady state. In the present simulations, the total forces agree with the sum of the individual component of fluid force through the sedimentation, especially Model B and C correspond to the numerical results in *Cases a* and *b*, respectively.

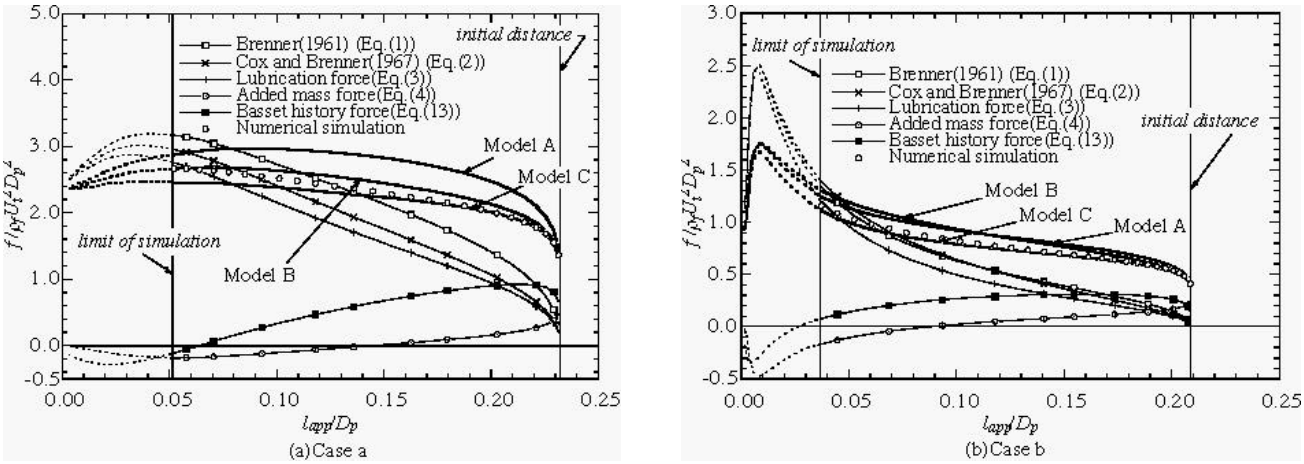

Fig.6 Steady and unsteady fluid forces and their linear models versus approach distance

CONCLUSIONS

A spherical solid particle approaching to the wall in an incompressible fluid under the gravity was studied. Both of numerical analyses and experiments were made to examine the fluid force models. In the numerical analyses, the fluid flow was solved by the moving boundary technique. Except for the close vicinity of the wall, the results of the numerical simulations, the experiments and the analyses using the theoretical models agreed quantitatively with respect to the falling motion of the particle. Furthermore, it was shown that the total force acting on the particle agreed with the sum of the individual component of fluid force through the sedimentation.

ACKNOWLEDGMENTS

This research was partially supported by the Japan Ministry of Education, Science, Sports and Culture, Grant-in-Aid for Scientific Research, No.10555060.

REFERENCES

Brady, J. F., Phillips, R. J., Lester, J.C. and Bossis, G., 1988, "Dynamic simulation of hydrodynamically interacting suspensions", *J. Fluid Mech.*, **195**, pp.257-280.

Sangani, A. S., Mo, G., Tsao, H. and Koch, D. L., 1996, "Simple shear flows of dense gas-solid suspensions at finite Stokes numbers", *J. Fluid Mech.*, **313**, pp.309-341.

Brenner, H., 1961, "The slow motion of a sphere through a viscous fluid towards a plane surface", *Chem. Eng. Sci.*, **16**, pp.242-251.

Cox, R. G. and Brenner, H., 1967, "The slow motion of a sphere through a viscous fluid towards a plane surface-II: Small gap widths, including inertia effects", *Chem. Eng. Sci.*, **22**, pp.1753-1777.

Adams, M. J. and Perchard, V., 1985, "The cohesive forces between particles with interstitial liquid", *Inst. Chem. Eng. Symp.*, **91**, pp.147-156.

Soo, S. L., 1967, *Fluid Dynamics of Multiphase Systems*, Blaisdell Publishing Company.

Briscoe, B.J. and Adams, M.J., 1987, *Tribology in Particulate Technology*, Adam Hilger.

Davis, R. H., Serayssol, J. and Hinch, E. J., 1986, "The elastohydrodynamic collision of two spheres", *J. Fluid Mech.*, **163**, pp.479-497.